

# Discovery of Diffuse Hard X-ray Emission around Jupiter with *Suzaku*

Y. Ezoe, K. Ishikawa and T. Ohashi

Department of Physics, Tokyo Metropolitan University, 1-1 Minami-Osawa, Hachioji,  
Tokyo 192-0397, JAPAN

ezoe@phys.metro-u.ac.jp

Y. Miyoshi

Solar-Terrestrial Environment Laboratory, Nagoya University, Furo-cho, Chikusa-ku,  
Nagoya 464-8601, JAPAN

N. Terada

Department of Geophysics, Tohoku University, 6-3 Aoba, Aramaki, Aoba-ku, Sendai,  
Miyagi 980-8578, JAPAN

Y. Uchiyama

Stanford Linear Accelerator Center, Stanford University, 2575 Sand Hill Road, Menlo  
Park, CA 94025, USA

and

H. Negoro

Department of Physics, Nihon University, 1-8-14 Kanda Surugadai, Chiyoda, Tokyo  
101-8308, JAPAN

Received \_\_\_\_\_; accepted \_\_\_\_\_

## ABSTRACT

We report the discovery of diffuse hard (1–5 keV) X-ray emission around Jupiter in a deep 160 ks *Suzaku* XIS data. The emission is distributed over  $\sim 16 \times 8$  Jovian radius and spatially associated with the radiation belts and the Io Plasma Torus. It shows a flat power-law spectrum with a photon index of  $1.4 \pm 0.2$  with the 1–5 keV X-ray luminosity of  $(3.3 \pm 0.5) \times 10^{15}$  erg s $^{-1}$ . We discussed its origin and concluded that it seems to be truly diffuse, although a possibility of multiple background point sources can not be completely rejected with a limited angular resolution. If it is diffuse, the flat continuum indicates that X-rays arise by the non-thermal electrons in the radiation belts and/or the Io Plasma Torus. The synchrotron and bremsstrahlung models can be rejected from the necessary electron energy and X-ray spectral shape, respectively. The inverse-Compton scattering off solar photons by ultra-relativistic (several tens MeV) electrons can explain the energy and the spectrum but the necessary electron density is  $\gtrsim 10$  times larger than the value estimated from the empirical model of Jovian charge particles.

*Subject headings:* planets and satellites: individual (Jupiter, Io) — X-rays: general

## 1. Introduction

In situ measurements and ground-based observations have shown the existence of Jupiter’s high-energy electron Van Allen radiation belts with evidence for electrons at energies of keV to 50 MeV (Berge & Gulakis 1976; Van Allen et al. 1975; Fischer et al. 1996; Bolton et al. 2002). Theoretically, electrons are energized by the betatron acceleration via the inward radial diffusion (Goertz et al. 1979; Miyoshi et al. 1999) and recently non-adiabatic acceleration via wave-particle interactions has been discussed (Horne et al. 2008). The trapped electrons lose their energy through synchrotron radio emission and some fraction are absorbed by Jovian moons and rings (Bagenal et al. 2004). However, there remains much debate over the precise energy spectrum and spatial distribution of the energetic electrons in the radiation belts.

Jupiter is the most luminous planet in the solar system at X-ray wavelength (Metzger et al. 1983; Waite et al. 1997; Bhardwaj et al. 2007). It emits X-rays from magnetic poles by the charge exchange interaction with the solar wind and magnetospheric heavy ions and also by the bremsstrahlung emission via energetic electrons (Gladstone et al. 2002; Branduardi-Raymont et al. 2004; Branduardi-Raymont et al. 2007a). A typical X-ray luminosity of the auroral emission is  $\sim 10^{16}$  erg  $s^{-1}$ . The low-latitude atmosphere also exhibits scattered radiation of solar X-rays with a typical luminosity of  $\sim 3 \times 10^{15}$  erg  $s^{-1}$  (Branduardi-Raymont et al. 2007b). Besides Jupiter itself, faint soft ( $< 1$  keV) X-rays from the Io Plasma Torus (IPT) have been detected ( $\sim 1 \times 10^{14}$  erg  $s^{-1}$ , Elsner et al. 2002). It may arise from bremsstrahlung emission by warm electrons with energies of few hundred to few thousand eV. Although we can expect hard X-rays ( $> 1$  keV) from energetic keV to MeV electrons in the Jupiter’s radiation belts, there has been no report on such an emission because past instruments lacked a necessary sensitivity to detect the extended hard X-ray emission. This indication motivated us to perform a decisive analysis using a deep 160 ks

observation data of Jupiter with *Suzaku*.

## 2. Observations

*Suzaku* (Mitsuda et al. 2007) observed Jupiter on 2006 February 24-28 with the X-ray Imaging Spectrometer (XIS) (Koyama et al. 2007). The XIS consists of three front-illuminated (FI) CCDs (XIS0, 2 and 3) and one back-illuminated (BI) CCD (XIS1).

Due to the low-earth orbit of *Suzaku* and the large effective area, the XIS-FI has the lowest particle background among all X-ray CCDs in currently available X-ray observatories. Figure 5 in Mitsuda et al. (2007) summarizes the background normalized by the effective area and the field of view, which is a good measure of sensitivity determined by background for spatially extended emission. The background of the XIS FI is the lowest among X-ray CCDs onboard *Suzaku*, *Chandra* and *XMM-Newton*. It is 2 and 5 times lower than the *XMM-Newton* MOS and pn, and *Chandra* ACIS-I in 2–5 keV, respectively. For this reason, we use only the XIS data in this paper.

During the observations, the spacecraft was repointed four times to allow for the planet’s motion (0.7~1.8 arcmin per day). The XIS was operated in the normal mode. The data reduction was performed on the version 2.0.6.3 screened data provided by the *Suzaku* processing facility, using the HEASoft analysis package ver 6.3.1. The net exposure of each FI and BI chip was 159 ks. For spectral fits, we generated response matrices and auxiliary files with `xisrmfgen` and `xissimarfgen`.

Although an optical loading from Jupiter (visual magnitude  $m_V = -2$  during *Suzaku* observations) often becomes a problem in X-ray observations (Elsner et al. 2002), we concluded that it is negligible in this case, because optical loading effects such as degradation of the energy resolution, changes in the energy scales and/or the detection

efficiency were not seen in XIS spectra. For confirmation, we estimated the optical blocking power of the XIS compared to CCDs onboard *XMM-Newton* (Lumb 2000). We found that the *Suzaku* XIS has almost the same blocking power as the *XMM-Newton* MOS with a thick filter, with which the observation of Jupiter was successfully conducted (Branduardi-Raymont et al. 2004).

### 3. Extended X-ray Emission

#### 3.1. Imaging analysis

To search for any emission from Jupiter, we have to remove *Suzaku*'s orbital motion and transform the data into Jupiter's comoving frame using an ephemeris obtained from the Jet Propulsion Laboratory (JPL). Before conducting this procedure, we checked X-ray images without these corrections. We created two-band mosaic images using XIS1 (BI) and XIS0+2+3 (FI) data as shown in figure 1. We corrected the data for positional difference in exposure times by using the exposure map generator `xisexpmapgen`. An extended emission is detected in both the 0.2–1 keV and 1–5 keV bands along the path of Jupiter.

Beside the extended emission, we found signatures of emission from point sources near Jupiter in the 1–5 keV band. Since we found no known point sources in the X-ray source catalogue compiled by NASA<sup>1</sup>, we decided to detect sources from the *Suzaku* image. We utilized the wavelet function program `wavdetect` in the CIAO package<sup>2</sup>. We created four 1–5 keV images with different bin sizes (1, 2, 4, and 8) and ran the point search program by setting the significant threshold above  $1 \times 10^{-6}$ , which corresponds to one spurious source in a  $1024 \times 1024$  pixel map (XIS field of view). We summarized source lists and removed

---

<sup>1</sup>[http://heasarc.gsfc.nasa.gov/cgi-bin/Tools/high\\_energy\\_source/high\\_energy\\_source.pl](http://heasarc.gsfc.nasa.gov/cgi-bin/Tools/high_energy_source/high_energy_source.pl)

<sup>2</sup><http://cxc.harvard.edu/ciao/>

possible spurious detections by visual inspection.

The obtained source positions are shown in figure 1 (b) (green circles with red lines). Twenty sources are detected with the 1–5 keV X-ray flux of  $1 \sim 3 \times 10^{-14}$  erg s<sup>-1</sup> cm<sup>-2</sup>. Here we converted a XIS count rate into flux, assuming a power-law spectrum with an photon index of 1.5 and an average absorption column toward this field<sup>3</sup>, which represents a typical spectrum of the background active galactic nucleus. This number is consistent with the canonical cosmic X-ray background model (Giacconi et al. 2001), which predicts 27 background sources above the detection limit. Although the source list contains marginally detected point sources, we decided to remove X-ray photons from the 1–5 keV image analysis afterward, for safety. We excluded circular regions with a diameter of 2 arcmin centered at individual sources. The diameter is equal to the beam size or the half power diameter of the XIS<sup>4</sup>. Since all the sources are faint, contamination from the sources is thus negligible. Because there are no significant point sources around Jupiter in the 0.2–1 keV image (fig. 1 a), we conducted this exclusion process only for the 1–5 keV image.

We then corrected the two-band images for *Suzaku*'s orbital motion and Jupiter's ephemeris. In case of the 1–5 keV image, to take into account the excluded regions, we created the exposure map for each observation and excluded the point source regions. Then we transformed the exposure map considering the Jupiter's orbit and divided the orbital motion corrected image by the corrected map. In case of the 0.2–1 keV image, we made the same analysis except for excluding the point source regions.

The results obtained are shown in figure 2. We detected a significant hard X-ray emission extended over  $\sim 16 \times 8 R_j$  which is positionally associated with the Jupiter's

---

<sup>3</sup><http://heasarc.gsfc.nasa.gov/cgi-bin/Tools/w3nh/w3nh.pl>

<sup>4</sup>[http://www.astro.isas.jaxa.jp/suzaku/doc/suzaku\\_td](http://www.astro.isas.jaxa.jp/suzaku/doc/suzaku_td)

radiation belts, and Io’s orbit. Because Io’s orbit coincides with the IPT, the emission is also spatially associated with the IPT. The X-ray luminosity of the extended emission arises from  $(3.6\pm 0.4)\times 10^{15}$  erg s<sup>-1</sup> and  $(3.3\pm 0.5)\times 10^{15}$  erg s<sup>-1</sup> in 0.2–1 and 1–5 keV, respectively. Here and below the uncertainties are 68 % confidence intervals. We assumed a distance to Jupiter of 5.0 AU on 24-28 Feb 2006. An estimated contamination of the point sources outside the excluded regions to the extended emission is  $\sim 20$  %. Hence, most of the emission is due to the extended component.

To check the distribution of the emission, we created projection profiles along the horizontal axis as shown in figure 3. The hard X-ray emission is significantly extended more than the point spread function (green line). We found that the profile can be roughly represented by a simulated model using `xissimarfgen`, which is a sum of a point source and a elliptical uniform emission with radii of 4 and 1.3 arcmin (12 and 4  $R_j$ ). The emission is thus extended over a wide region ( $> 6 R_j$ ). On the other hand, the soft emission is marginally consistent with the point source. There is an excess on the right side of the soft X-ray peak, which suggests emission from the IPT that has been reported by Elsner et al. (2002).

The hard X-rays are hence unlikely to originate only from a single point source or Jupiter. Furthermore, an artificial effect on the extended morphology due to the analysis can be excluded because of the different morphology from the soft X-ray image. The emission thus seems to contain truly diffuse component related to Jovian magnetospheric processes.

We note that the faintness of the emission should have hindered its detection in the past observations. Considering the angular resolution of *XMM-Newton*, its surface brightness will be  $1/30\sim 1/40$  of Jupiter’s aurora, From figure 5 in Branduardi-Raymont et al. (2007a), we can roughly estimate the CCD background level as  $1/10$  of the auroral

emission. Therefore the detection of the diffuse emission should be quite difficult. If the emission is related to Jovian radiation belts, there can be also time variation (see §4).

### 3.2. Spectral analysis

To investigate characteristics of the emission, we analyzed its X-ray spectrum by extracting photons around the extended emission region. For simplicity, we excluded the point sources from the event files without orbital motion corrections and extracted events from a circular region with a radius of 3 arcmin centered at the path of Jupiter. The surrounding region with an outer radius of 6 arcmin after subtracting the point sources was utilized as a background. Consequently, this extended emission region includes both Jupiter and the extended emission, because the limited angular resolution hindered us to spatially separate these two components.

Figure 4 shows the spectrum obtained. It consists of a flat continuum extending up to 5 keV and signs of lines around 0.25 keV and 0.56 keV. Hence, we fitted the spectrum with a power-law plus two Gaussian model. The best-fit model represents data well with  $\chi^2/\nu \sim 0.5$ . No absorbing column was required, as expected from the source's proximity. The obtained photon index was  $1.4 \pm 0.2$ , while the central energies of the two Gaussian were  $0.24 \pm 0.1$  keV and  $0.56 \pm 0.1$  keV. Fluxes for the 0.24 keV and 0.56 keV lines were  $(3.9 \pm 0.6) \times 10^{-5}$  and  $(2.0 \pm 0.5) \times 10^{-5}$  photons  $\text{cm}^{-2} \text{s}^{-1}$ , respectively.

Characteristics of the two lines such as a central energy and a flux were similar to those of the Jupiter's auroral emission observed with *XMM-Newton* in Nov 2003 (see table 3 in Branduardi-Raymont et al. 2007a). The two lines at 0.24 keV and 0.56 keV are presumably a line complex from  $\text{C}^{5+}$  and ionized Mg, Si, S and a  $\text{K}_\alpha$  emission from  $\text{O}^{6+}$ , respectively. Such line emissions are distinct features of the charge exchange reaction



(Cravens et al. 2003). Taken together with the fact that the 0.2–1 keV X-rays arise from a compact region near Jupiter, most of soft X-rays likely originate from Jupiter’s aurora via the charge exchange.

In contrast, the 1–5 keV X-ray emission was represented by a simple flat continuum with a photon index of 1.4. Since the peak of the X-rays coincides with Jupiter (fig. 2 b), some fractions of the emission can arise from Jupiter.

The power-law spectrum was in fact seen in the past *XMM-Newton* observations of Jupiter’s aurora (Branduardi-Raymont et al. 2004). For comparison, we plotted auroral emission models in three past *XMM-Newton* observations (tables 2 and 3 in Branduardi-Raymont et al. 2007a) in figure 4. The 1–5 keV fluxes of these models are smaller than that of the *Suzaku* best-fit model by a factor of 2~3. This is consistent with an independent estimation from the projection profile that most of the extended emission comes from diffuse emission other than Jupiter.

#### 4. Discussion

We have discovered extended hard X-ray emission around Jupiter. Although its spatial association with Jupiter strongly suggests a diffuse component related to Jovian magnetospheric processes, we first have to examine serendipitous background sources. Because we corrected the image for the Jupiter’s orbital motion, any faint background source on the Jupiter’s path, that is missed in our point source identification procedure, can be seen as extended emission in the orbital motion corrected image. Considering the almost symmetric projection profile (fig. 3) centered at Jupiter, the spatial distribution of the background sources should be symmetric about Jupiter. The most plausible case is that the emission is composed of Jupiter itself and a single background point source near the center

of the Jupiter’s orbit. To test this hypothesis, we excluded the central part of the Jupiter’s orbit with a circle region in the same way as figure 1 (b), and created the orbital motion corrected image and projection profile in 1–5 keV. We still observed a significant extended emission around Jupiter, although the total count rate decreased by  $\sim 15\%$ . Hence, a single background source cannot fully explain the observed emission. Since multiple point sources with symmetric spatial distribution against Jupiter are less probable, below we discuss the origin of the emission, considering that the emission is truly diffuse.

The flat power-law continuum of the emission suggests a non-thermal mechanism. There are three candidates for the emission mechanism; synchrotron emission, bremsstrahlung emission, and inverse-Compton scattering. The synchrotron interpretation can be easily rejected in terms of the required electron energy. From the X-ray image, we can observe the hard X-rays at the Io’s orbital plane (a distance from Jupiter,  $r = 5.9 R_j$ ) or even more distant area. At  $r \sim 6 R_j$ , the magnetic field of the Jovian magnetosphere is quite weak on the order of 0.01 G. With such a weak magnetic field, if we want to generate synchrotron emission in the X-ray wavelength range, TeV electrons are necessary. This energy is more than  $10^4$  times higher than the observed maximum electron energy in the radiation belts ( $\sim 50$  MeV) (Bolton et al. 2002). Even if TeV electrons exist, their Larmor radius ( $3 \times 10^{11}$  cm for 1 TeV electron at  $r = 6 R_j = 4 \times 10^{10}$  cm) will be too large, so that TeV electrons are not trapped in the magnetic field line and will escape from the Jupiter’s radiation belts.

The bremsstrahlung emission is possible in terms of the electron energy, because we need only keV electrons which have been observed in the past in-situ measurements (Bagenal et al. 2004). Such electrons will interact in an ambient medium and produce not only continuum but also X-ray lines by collisional excitation and inner-shell ionization (see §3.1 in Tatischeff 2002). From in-situ measurements, the plasma at  $r \sim 6 R_j$  is known to be mainly composed of heavy ions such as  $S^+$  and  $O^+$  (see fig. 23.2 in Bagenal et al. 2004).

We estimated an equivalent width of S  $K_\alpha$  line (2.3 keV). We used cross sections for K-shell ionization by electron impact from Santos et al. (2003) and the bremsstrahlung loss rate of electrons given by Skibo et al. (1996), to estimate the line and continuum intensities, respectively. The calculated equivalent width of the S  $K_\alpha$  line was as large as  $\sim 10$  keV, which should be observed in the XIS spectrum with the good energy resolution ( $\sim 130$  eV at 6 keV, Koyama et al. 2007). As shown in figure 4, no such line exists around 2 keV. Hence, the bremsstrahlung interpretation can be rejected.

The remaining possibility is inverse-Compton scattering. We consider the scattering of solar light by ultra-relativistic electrons in the radiation belts. In this process, the scattered photon energy will be

$$\sim 8 \text{ keV} (E_{\text{ph}}/1.4 \text{ eV}) (E_e/50 \text{ MeV})^2, \quad (1)$$

where  $E_{\text{ph}}$  is an energy of solar optical photons and  $E_e$  is that of relativistic electrons (Rybiki & Lightman 1979). Considering the maximum observed electron energy of 50 MeV in the inner radiation belts (Bolton et al. 2002), the inverse-Compton scattering is possible in terms of the electron energy. Although 50 MeV electrons have not been observationally well confirmed at outer regions ( $r >$  several  $R_j$ ), there may exist such ultra-relativistic electrons in these regions as expected from the empirical model (e.g., Divine & Garret 1983). Also, since this mechanism does not need the emission line, the observed spectral shape can be safely explained.

Assuming the inverse Compton scattering, we can estimate the index of the electron number density spectrum as  $\sim 2$ , from the photon index of the X-ray spectrum (Rybiki & Lightman 1979). This is consistent with the Divine-Garrett (DG) empirical charged particle model of Jovian magnetosphere (Divine & Garret 1983) ( $\sim 3$  at 6  $R_j$ ) and another model based on the *Galileo* data (Garret et al. 2003) ( $\sim 3$  at 8  $R_j$ ).

We then proceeded to estimate the necessary electron number density. For simplicity,

we assumed that the emission region is an oblate spheroid with radii of 8, 8, and 4  $R_j$ , and the monotonic electron energy of 50 MeV. We here considered anisotropic angular distribution of the inverse-Compton scattering (Brunetti et al. 2001). During the *Suzaku* observation, the Sun-Jupiter-Earth angle was  $10^\circ$ . Because of the larger cross section of the back scattering, the inverse-Compton flux will increase by a factor of  $\sim 3$ . The estimated average electron number density to explain 80% of the hard X-rays was  $\sim 0.005 \text{ cm}^{-3}$ .

For comparison, we utilized the DG empirical model, which provides a theoretical electron spectrum as a function of the distance from Jupiter. The DG model is based on the data taken with *Pioneer* and *Voyager*. To date, it is the best model to estimate the MeV electron distribution in the inner radiation belts ( $< 8 R_j$ ). We found that the  $> 20$  MeV electron number density is only  $\sim 0.0007$  and  $0.0001 \text{ cm}^{-3}$  at 4 and 6  $R_j$ , respectively. The density will decrease as the distance increases. Hence, there is a factor of 7~50 discrepancy. Although the situation can be somewhat relaxed by an uncertainty of the DG model (Bolton et al. 2001) and/or time variations of the trapped MeV electrons (Miyoshi et al. 1999; Bolton et al. 2002; Santos-Costa et al. 2008), this interpretation needs further investigations.

In conclusion, further X-ray, radio and in-situ observations are necessary to understand the origin of this diffuse hard X-ray emission, to identify the emission region with the Jupiter’s magnetosphere, the IPT and/or else, and to clearly distinguish the emission from background point sources.

## REFERENCES

- Bagenal, F., Dowling, T.E., & McKinnon, W.B. 2004, *Jupiter: The Planet, Satellites and Magnetosphere* (Cambridge University Press).
- Berge, G. L. & Gulkis, S. 1976, *Jupiter* (ed. Gehrels, T.; Univ. Arizona Press).
- Bhardwaj, A., et al. 2007, *Planetary Space Sci.*, 55, 1135.
- Bolton, S. J., et al., 2001, *Geophys. Res. Lett.*, 28, 907.
- Bolton, S. J. et al. 2002, *Nature* 415, 98).
- Branduardi-Raymont, G. et al. 2004, *A&A*, 424, 331.
- Branduardi-Raymont, G. et al. 2007a, *A&A*, 463, 761.
- Branduardi-Raymont, G. et al. 2007b, *Planetary Space Sci.*, 55, 1126.
- Brunetti, G., Cappi, M., Setti, G., Feretti, L., & Harris, D. E. 2001, *A&A*, 372, 755
- Creavens, T.E., 2003, *J. Geophys. Res.*, 108, 1465.
- Divine, N., & Garret, H.B. 1983, *J. Geophys. Res.*, 88, 6889.
- Elsner, R.F. et al. 2002, *ApJ*, 572, 1077.
- Fischer, H. M., Pehlke, E., Wibberenz, G., Lanzerotti, L. J. & Mihalov, J. D. 1996, *Science* 272, 856.
- Giacconi, R. et al., 2001, *ApJ*, 551, 624.
- Garret, H.B. et al, 2003, NASA/JPL publication 03-006.
- Gladstone, G.R. et al. 2002, *Nature*, 415, 1000.

- Goertz, C. K., J. A. Van Allen, & M. F. Thomsen, 1979, *J. Geophys. Res.*, 84, 87.
- Horne, R.B. et al. 2008, *Nature Physics* 4, 301.
- Koyama, K. et al. 2007, *PASJ*, 59, S23.
- Lumb, D. 2000, XMM PHS Tools - EPIC Optical loading.
- Metzger, A.E. et al. 1983, *J. Geophys. Res.*, 88, 7731.
- Mitsuda, K. et al. 2007, *PASJ*, 59, S1.
- Miyoshi, Y., et al. 1999, *Geophys. Res. Lett.*, 26, 9.
- Rybiki, G.B., & Lightman, A.R. 1979, *Radiative Processes in Astrophysics* (A Wiley-Interscience Publication).
- Santos, J.P., Parente, F., & Kim, Y-K. 2003, *J. Phys. B: At. Mol. Opto. Phys.*, 36, 4211.
- Santos-Costa, D., et al., 2008, *J. Geophys. Res.*, 113, A01204.
- Serlemitsos, D., et al., 2007, *PASJ*, 59, S9.
- Skibo, J.G., Ramaty, R., & Purcell, W.R. 1996, *A&AS*, 120, 403.
- Tatischeff, V., 2002, [astro-ph/020839](#).
- Uchiyama, Y. et al., 2008, *PASJ*, 60, S35.
- Van Allen, J. A., Baker, D. N., Randall, B. A. & Sentman, D. D. 1975, *Science*, 188, 459.
- Waite Jr., J.H. et al. 1997, *Science*, 276, 104.

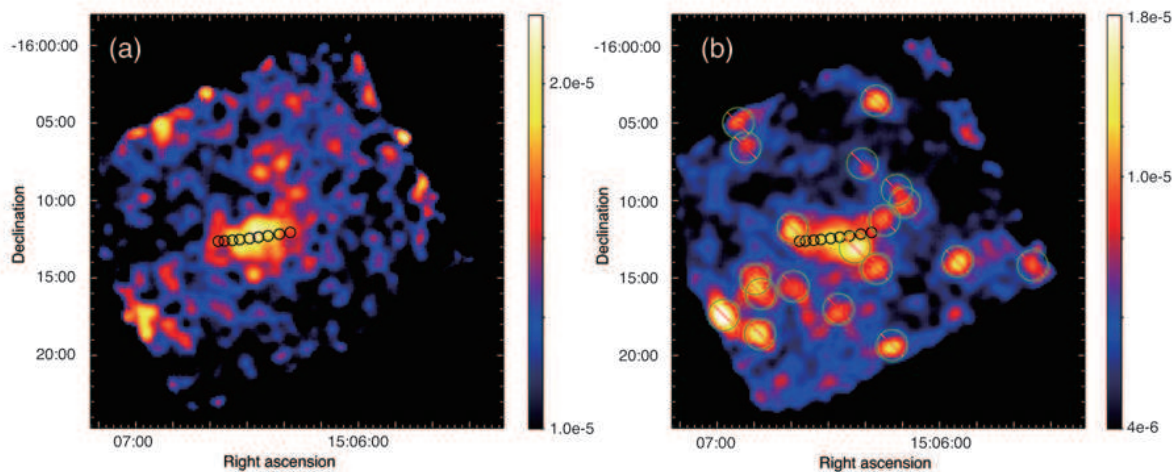


Fig. 1.— *Suzaku* XIS mosaic images of the vicinity of Jupiter in the (a) 0.2–1 keV (BI) and (b) 1–5 keV (FI) bands, displayed on the J2000.0 coordinates. Exposures are corrected and the count unit is counts  $\text{s}^{-1}$  binned  $\text{pixel}^{-1}$ . For clarity, images are binned by a factor of 8 and smoothed by a Gaussian of  $\sigma = 5$  pixels. Black circles show the size and position of Jupiter during the observations. Considering known pointing uncertainty of *Suzaku* (Uchiyama et al. 2008), positions of the circles are slightly shifted by +25 and  $-25$  arcsec in the Ra and Dec directions, respectively, in order that the extended emission coincides with the Jupiter’s path. Green circles with red lines mark excluded point source regions when we create the 1–5 keV image in comoving frame (see text).

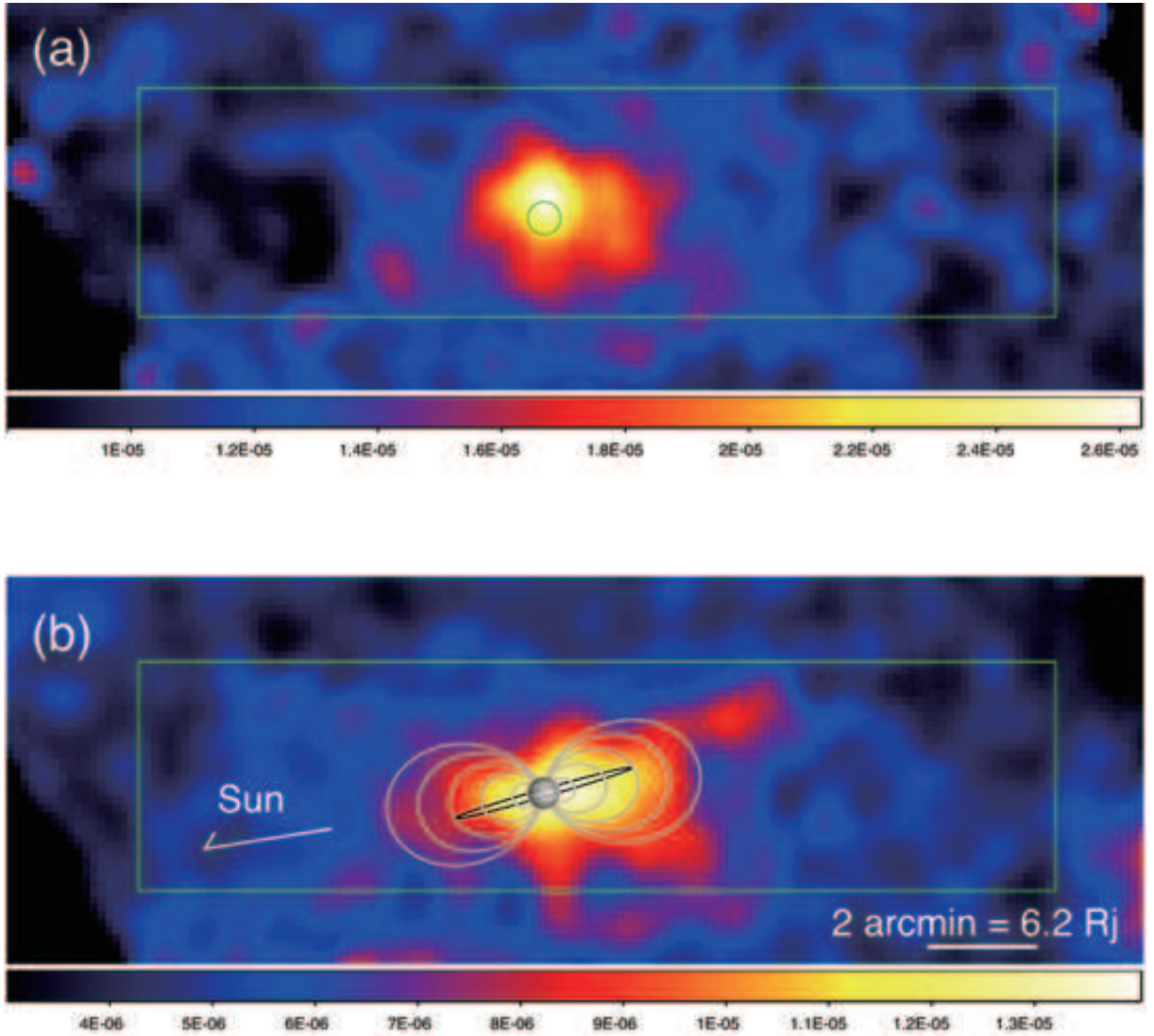


Fig. 2.— *Suzaku* XIS images after correcting for the satellite’s orbital motion and Jupiter’s ephemeris in the (a) 0.2–1 keV (BI) and (b) 1–5 keV (FI) bands. The images are binned and smoothed in the same way as figure 1. In the panel (a), a circle indicates the expected position and size of Jupiter whose diameter is 39 arcsec. In the panel (b), grey lines indicate the equatorial crossing of magnetic field lines at 2, 4, 6, and 8 Jovian radius ( $R_j$ ). A black line is the path traced by Io. A photograph of Jupiter by *Cassini* taken from the JPL web site is overlaid. An arrow indicates the direction of the Sun. Boxes are used to obtain the projection profiles in figure 3.



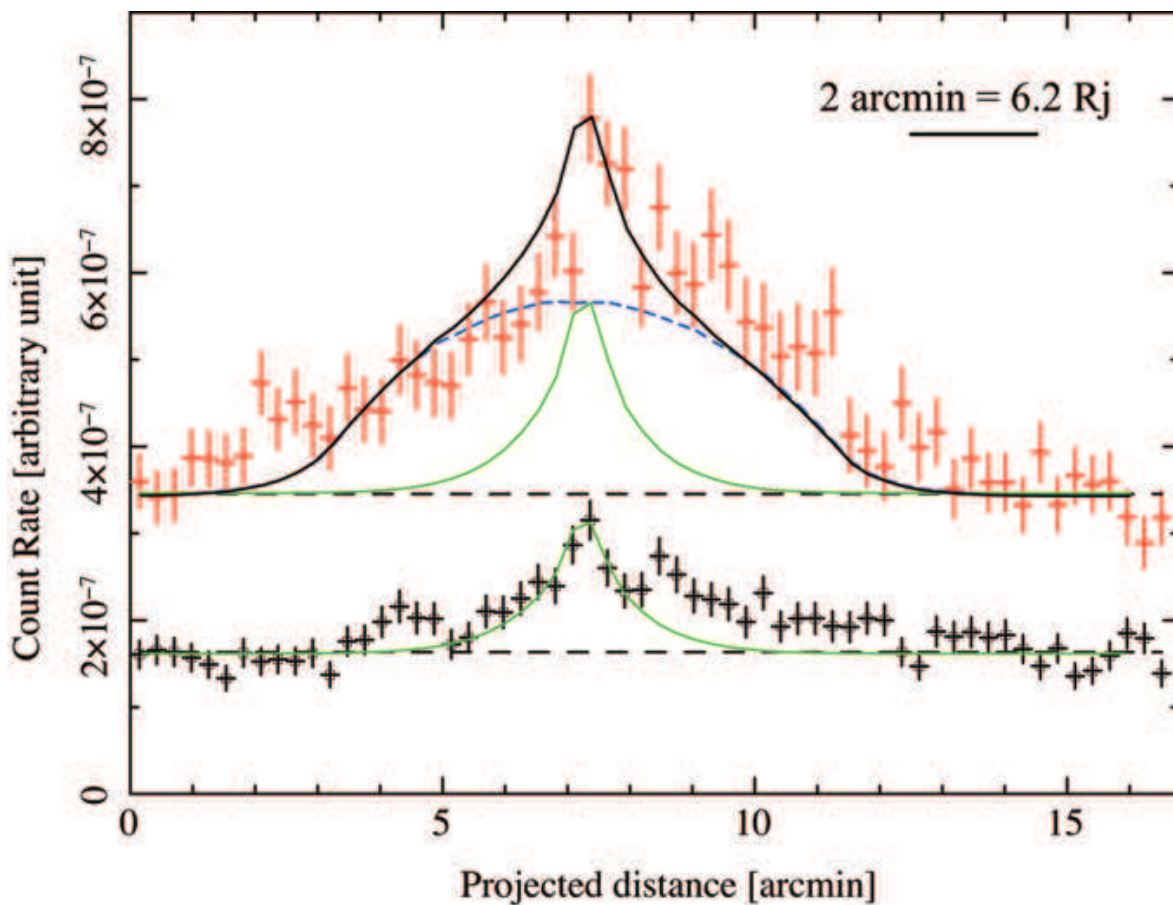


Fig. 3.— Projection profiles along the horizontal axis, extracted from box regions in figure 2. Black and red points show the 0.2–1 and 1–5 keV data, respectively. Errors are  $1\sigma$  statistical ones. Green lines are a simplified model of Jupiter’s X-rays (42 arcsec diameter) in the two energy bands, whose normalization and offset are tuned to coincide with the profile. The point spread function is almost the same at different energies (Serlemitsos et al. 2007). A dashed blue line indicates the expected profile of an uniform emission extended over an elliptical region with radii of 4 and 1.3 arcmin. A solid black line is the sum of the dashed green and blue lines. Dashed black lines are background levels estimated by fitting the data above the projected distance  $>14$  arcmin with a constant.

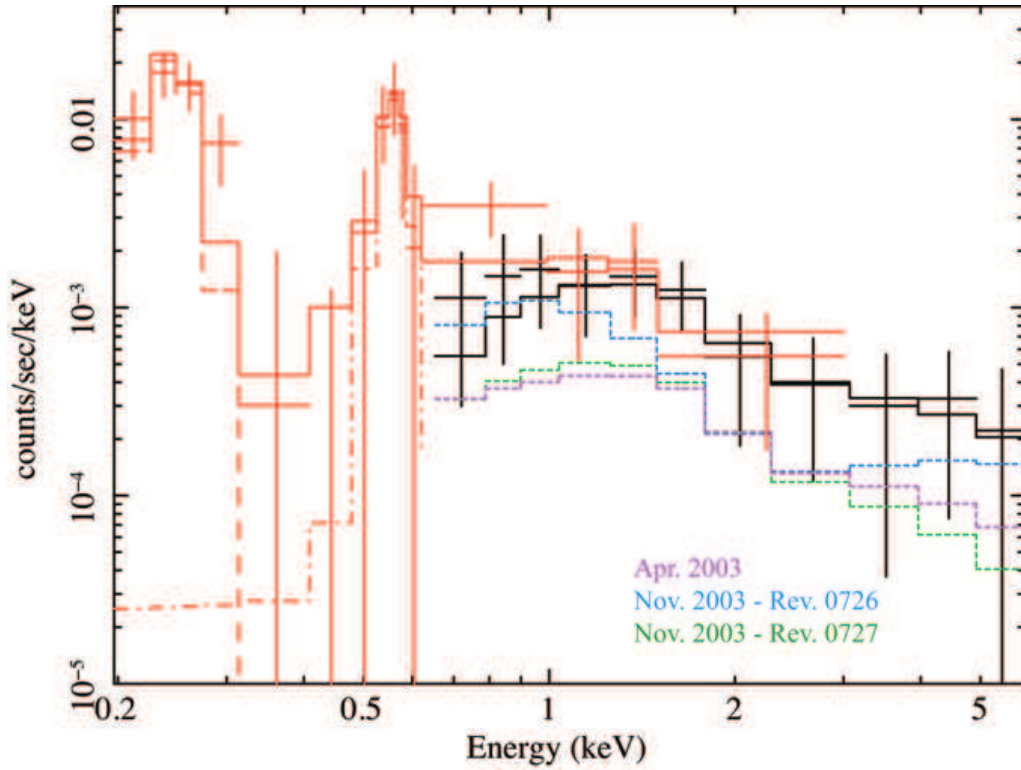


Fig. 4.— Background subtracted BI (red) and FI (black) spectrum of the extended emission region, compared with the best-fit power-law plus two Gaussian models (solid line). Two Gaussians are shown in dashed and dash-dotted lines. Purple, green and blue dashed lines plotted for the FI spectrum are Jupiter’s auroral continuum emission models in *XMM-Newton* observations (Branduardi-Raymont et al. 2007a).